

Article

Research on the Experimental System of Reinforcing the Base of Shallow Buried and Wet Collapsible Loess Tunnels

Zhiqiang Li ¹, Shixin Lv ¹, Jinpeng Zhao ¹, Lulu Liu ^{1,2,3,*} and Kunkun Hu ¹

¹ School of Civil Engineering, Weifang University, Weifang 261061, China; 20111484@wfu.edu.cn (Z.L.); lxx1052332819@163.com (S.L.); peng19_98@163.com (J.Z.); kunhkun@163.com (K.H.)

² School of Highway, Chang'an University, Xi'an 710064, China

³ State Key Laboratory for Geomechanics and Deep Underground Engineering, China University of Mining and Technology, Xuzhou 221116, China

* Correspondence: believeliululu@163.com or liululu@cumt.edu.cn; Tel.: +86-186-5161-1376

Abstract: Due to the complexity of the surrounding rock structure and the geological environment of tunnel excavations, traditional analytical methods are insufficient in effectively dealing with the complex nonlinear deformation problems arising from tunnel excavation. In contrast, geomechanical model tests can comprehensively simulate the excavation construction process of tunnels and the mode and time effects of loads, providing a more realistic reflection of the complete process of engineering stress and deformation. Therefore, this study conducted a model test on reinforcing the loess tunnel base, building upon the first tunnel of the Lanqing Expressway located on the north bank of the Yellow River in Lanzhou City. The study utilized similarity theory to explore the theoretical design of the model and established a specialized model test platform to design the experiments with the goal of obtaining more scientific and effective experimental schemes to ensure the safety of soil reinforcement in tunnel bases during construction. This research will contribute to improving the safety, reliability, and economy of loess tunnel base reinforcement projects, and has a certain reference value for research in this field.

Keywords: loess tunnel; foundation reinforcement; similarity theory; model test design



Citation: Li, Z.; Lv, S.; Zhao, J.; Liu, L.; Hu, K. Research on the Experimental System of Reinforcing the Base of Shallow Buried and Wet Collapsible Loess Tunnels. *Buildings* **2023**, *13*, 1740. <https://doi.org/10.3390/buildings13071740>

Academic Editor: Hany El Naggar

Received: 19 May 2023

Revised: 29 June 2023

Accepted: 7 July 2023

Published: 10 July 2023



Copyright: © 2023 by the authors. Licensee MDPI, Basel, Switzerland. This article is an open access article distributed under the terms and conditions of the Creative Commons Attribution (CC BY) license (<https://creativecommons.org/licenses/by/4.0/>).

1. Introduction

With the large-scale development of western cities, rail transportation inevitably passes through wet collapsible loess areas. Considering the special engineering properties of the wet collapsible loess and the large number of traffic loads that the upper part of the tunnel bears, it is likely to cause a series of engineering disasters such as cracks, misalignments, and water and sand inrush in the tunnel after operations. Therefore, reasonable tunnel reinforcement measures are particularly necessary.

Currently, research on reinforcement measures for loess tunnels mainly focuses on tunnel surrounding rock pressure, lining structure calculations, and construction techniques. Most of these studies use theoretical analysis and numerical simulation methods. For example, Shao, S. et al. (2021) used numerical simulations to simulate the structural properties, strata, geological conditions, and excavation support effects of loess, analyzing and revealing the formation mechanisms of different types of failures during the construction process of loess tunnels [1]. Qiu, J. et al. (2022) used a comprehensive method combining theoretical derivation and numerical simulation to study the response mechanism of loess subway tunnels under partial water environments [2]. Cheng, X. et al. (2017) studied the influence of seepage on the seismic response of loess tunnels using ADINA to simulate the structural field and fluid field, compared and analyzed the maximum principal stress, minimum principal stress, lining maximum displacement, and internal forces of the tunnel structure, and further obtained the influence of rainwater seepage on the mechanical properties of LTSLs [3]. Weng, X. et al. (2021) used numerical simulations to study the effects of different

flooding methods on tunnel linings and further studied the stress and deformation of tunnel linings, strata, and surface subsidence after local soil collapse in the tunnel, as well as the mechanical mechanisms causing these effects [4]. In order to investigate the potential damage of shallowly buried multi-support underground structures during earthquakes, Zucca, M. and Valente, M. (2020) conducted extensive numerical simulations and evaluated the seismic performance of various structural configurations [5]. In addition, Xue, Y. et al. (2020) obtained a representative data sample set of total deformation in loess tunnels using numerical simulation methods and could effectively predict the total deformation of typical loess tunnels using a backpropagation neural network (BPNN) [6]. Hongtao, N. et al. (2022) used the finite difference software FLAC3D to simulate and analyze three-dimensional modeling numerical calculations under the construction conditions of upper and lower step excavation for the technical problems of tunnel excavation under special stratum conditions of loess-covered soil–rock contact zones and analyzed the rock failure characteristics of the contact zone surrounding rock from multiple aspects [7]. Moreover, in the machine learning applications in geomechanics, Savvides, A.-A. and Papadopoulos, L. (2022) have proposed a set of feed forward neural networks to estimate the stresses and strains at failure for cohesive soils subjected to loads from shallow foundations [8]. Furthermore, Sun, Z. et al. (2022) comprehensively described the deformation characteristics of tunnels crossing through loess-bedrock strata through numerical simulations and discussed in detail the mechanical behavior and displacement effects of cyclic loads on tunnels and sliding surfaces [9]. Mao, Z. et al. (2019) used the MIDAS geotechnical analysis system to simulate the construction process of a navigation tunnel and bilateral guide tunnels in a loess multi-arch tunnel, and studied the changes in surrounding rock stress and seepage fields during the construction process of the loess multi-arch tunnel [10]. Liu, Y. et al. (2017) simulated the strain–stress behavior of loess using the Duncan–Zhang EB model and studied the deformation and mechanical properties of tunnel linings under different flooding conditions [11].

Currently, there is still a lack of clear theoretical support for research on foundation stress and deformation in tunnel engineering, and design personnel mainly rely on subjective engineering experience to design reinforcement schemes for tunnel bottoms. In other soft rock tunnel foundation reinforcement designs, the processing methods used lack a rigorous theoretical basis. Therefore, it is necessary to conduct in-depth research on tunnel surrounding rock stability and support control to ensure the construction and excavation of tunnels in loess areas and safe operation in the later stages. However, due to the complexity of the tunnel surrounding rock structure and geological environment, traditional theoretical analytical solutions have difficulty handling these complex nonlinear deformation problems related to tunnel excavation. At the same time, considering that numerical analysis still faces difficulties in simulating underground engineering strength failure, geological model experiments have become a better choice. Geological model experiments can better simulate the excavation construction process of tunnels and the effects of load application and time effects and can reflect the complete process of engineering stress deformation more realistically.

Experts led by Fumagalli (2013) pioneered engineering geological model test technology at the Italian Structural Model Test Center, followed by extensive research by many scholars [12]. Fan, H. et al. (2023) analyzed the mechanical properties and deformation characteristics of tunnel linings for reinforced jet grouting piles in loess tunnel foundations and the impact of changes in pile geometry on tunnel foundation stability using centrifugal model tests and numerical simulations [13]. Cheng, X. et al. (2021) established a dynamic model and a rainwater infiltration model for loess two-lane tunnels considering the coupled effects of seismic activity, rainfall infiltration, and traffic movements. Using near-field pulse seismic excitation, the influence of loess tunnel seepage, traffic loads, and seismic activity on the driving dynamic response of loess tunnels was studied [14]. Qiu, J. et al. (2020) designed model tests according to different water source locations and tunnel lining forms, studied the collapsibility of loess under a high-pressure water environment and the failure

behavior of subway tunnels, and analyzed the distribution laws of tunnel water pressure field, displacement field, and stress field [15]. Cheng, X. et al. (2020) established four different section tunnel models and combined them with fluid models to study rainwater leakage, earthquakes, and train-induced effects, further analyzing the displacement, stress, and pore water pressure of loess tunnel critical points, and obtained the dynamic response mode of loess tunnels under the action of earthquake, rainwater infiltration, and train loads [16]. Lai, H. et al. (2019) first studied ground subsidence caused by loess tunnel construction through a uniquely designed centrifuge model test and proposed a new method that considers the special engineering characteristics of loess to evaluate the construction settlement of loess tunnels [17]. Fan, H. et al. (2023) analyzed the settlement of tunnel bedrock and the structural mechanical response characteristics under the influence of jet grouting piles with different lengths and diameters in weak loess areas using centrifugal model tests, effectively reducing tunnel bottom settlement and significantly shortening the stress adjustment time of surrounding rocks [18]. Yang, T. et al. (2020) established a precise grouting reinforcement test system, using the Yuhang Road tunnel with overlying loess as the injection medium, and conducted an orthogonal test based on slurry dry density, moisture content, water–cement ratio, and grouting pressure [19].

Based on the #1 tunnel of the Lanzhou–Qinhuangdao Expressway on the north bank of the Yellow River in Lanzhou City, this paper conducts a model test for the reinforcement of loess tunnel foundations. Similarity theory is used to theoretically study the design of the model, aiming to obtain a more scientific and specific experimental plan for the project to ensure the safety of the reinforcement of loess tunnel foundations in engineering.

2. Test Purpose and Simulated Working Conditions

2.1. Supporting Projects

The #1 tunnel of the Lanzhou–Qinhuangdao Expressway has a total length of 802 m, with a maximum depth of 112 m and a minimum depth of 20 m. The research object selected is the shallow section of 20 m, with a class V surrounding rock along the full length. The tunnel passes through a loess ridge, with the entrance located on the side of a loess gully and the exit on the right side of the upstream mountain of the Qiujia Gully. The excavation span of the tunnel is 17 m, with a height of 11 m, and it belongs to a special large-section loess tunnel with three lanes.

The collapsible loess in the tunnel site area is developed and has a large thickness. Figure 1 shows the longitudinal profile of the tunnel.

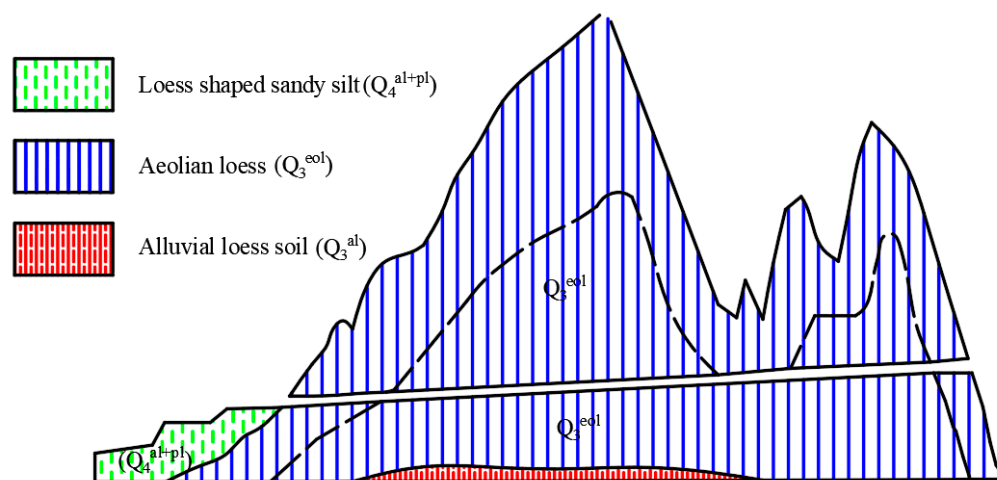


Figure 1. Longitudinal section of tunnel.

The entire base of the Fujia Tunnel is reinforced with high-pressure rotary jet grouting piles, with a pile diameter of 0.6 m, a pile length of 6 m, a pile spacing of 1.2 m, and a clover-shaped pile arrangement. Through on-site static load tests, it is determined that the bearing

capacity of the composite foundation after reinforcement should reach at least 300 kPa, with a designed cement content of 15%. The rotary jet grouting piles are constructed before the excavation of the tunnel's upward arch, and after finishing, the excavation of the upward arch is carried out. Figures 2 and 3 show the plan layout and on-site construction of the rotary jet grouting piles, respectively.

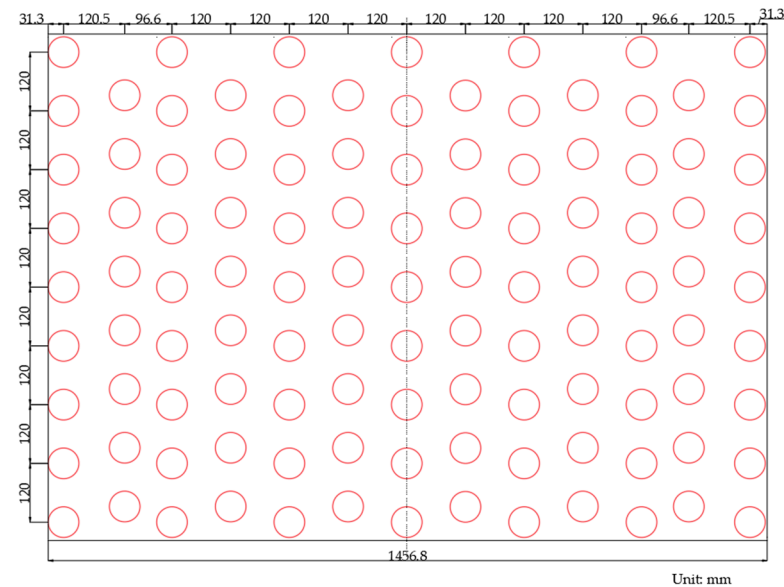


Figure 2. Plan arrangement diagram of piles.



Figure 3. On-site construction diagram of the tunnel-based jet grouting pile.

2.2. Test Purpose and Simulated Working Conditions

2.2.1. Test Purpose

The main purpose of this model test is to simulate various working conditions of the Fujia Tunnel, measure the displacement of the surrounding soil, the contact pressure between the lining and the surrounding rock, the vertical displacement of the tunnel support structure, the stress in the side walls and base soil, and the internal displacement of the base soil. It analyzes the force and deformation laws of the support structure system, especially the contact pressure at the bottom of the upward arch and the stress and deformation in the base soil, and simulates the adaptability of the current rotary jet grouting pile reinforcement technology based on these analyses. In addition, considering

that loess undergoes significant deformation when exposed to water, the test also considers the immersion condition. The contact pressure between the lining and the surrounding rock, the stress in the side walls and the base soil, the displacement of the base soil, the pressure at the top of the piles, and the soil pressure between them are measured under immersion conditions in order to analyze the force and deformation characteristics of the composite base under the upward arch. Finally, based on this research, a reasonable evaluation is made of the adaptability of the rotary jet grouting pile reinforcement technology.

2.2.2. Test Plan

This article mainly simulates two working conditions: condition 1, in which the tunnel uses a natural base, and condition 2, in which the tunnel's base is treated with high-pressure rotary jet grouting piles. As the water content of the surrounding rock gradually changes, the aim is to study the force and deformation of the tunnel support structure system and the force and deformation characteristics of the composite base under the upward arch. Please refer to Table 1 for specific details.

Table 1. Indoor model test plan for loess tunnel.

Shallow Burial (20 m)	Different Working Conditions	Test Substrate Status	Simulated Working Conditions
Condition 1	Natural substrate	Base undisturbed	The contact pressure at the bottom of the loess tunnel invert, and stress and deformation in the foundation soil
		Base humidification	Contact pressure at the bottom of the arch, stress and deformation in the foundation soil
Condition 2	High-pressure rotary jetting pile foundation	Base undisturbed	Stress and deformation characteristics of the composite foundation under the arch
		Base humidification	Stress and deformation characteristics of the composite foundation under the arch

2.2.3. Excavation Method and Immersion Method

Excavation was carried out manually due to the low strength of the surrounding rock. According to the construction method in the shallow buried section on site, the CD method was used for excavation, as shown in Figure 4. During the excavation and support process, the displacement field and stress field of the similar materials were monitored in real time. Excavation of the next cycle could only be carried out after the stress deformation became stable. Since each intermediate plate was 20 cm long and based on the tunnel's actual excavation conditions, the right upper heading was excavated 10 cm ahead of the left upper heading, and the right upper heading was excavated 20 cm ahead of the right lower heading, with a geometric similarity ratio of 40. When converted to the actual engineering conditions, the right upper heading was excavated 4 m ahead of the left upper heading, and the right upper heading was excavated 8 m ahead of the right lower heading. Two cycles were excavated every day, with each cycle excavating 5 cm. The left upper heading was excavated through on the 11th day, and after that, four cycles were excavated per day. The shield was removed when the left lower heading was excavated to 20 cm, 40 cm, 60 cm, 80 cm, and 100 cm. The total excavation period was 12 days.

2.2.4. Test Content and Location

The data for this test were collected using the DH3820Net static strain testing system. The strain gauge testing used a $\frac{1}{4}$ bridge connection, while the pressure box testing used a full bridge connection. The sampling frequency was set to 1 Hz. After connecting the wiring, the device was connected to a computer, and the switch on the collector was turned on. After following the steps of searching for the chassis, balancing, frequency setting, and bridge selection, the data collection was carried out.

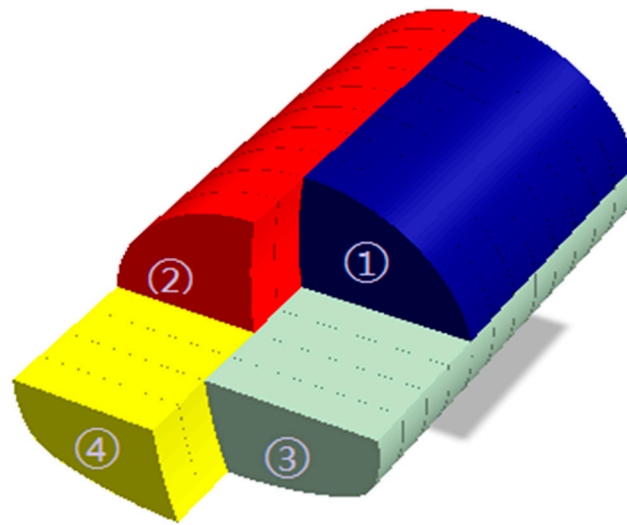


Figure 4. Schematic diagram of CD method excavation.

Through studying the changes in contact pressure between the tunnel lining and the surrounding rock, especially the contact pressure at the upward arch, as well as the stress and deformation changes in the lower soil, this model test explores specific measures for the treatment of the tunnel foundation, providing data for research on rational methods of tunnel foundation treatment. The test content includes:

- (1) Radial displacement around the cavern

Strain gauge measuring points were set up at the crown, mid-point of the upward arch, side walls, and locations with large displacement at the wall base, as shown in Figure 5. The measurement was conducted using a strain gauge with an accuracy of one percent.

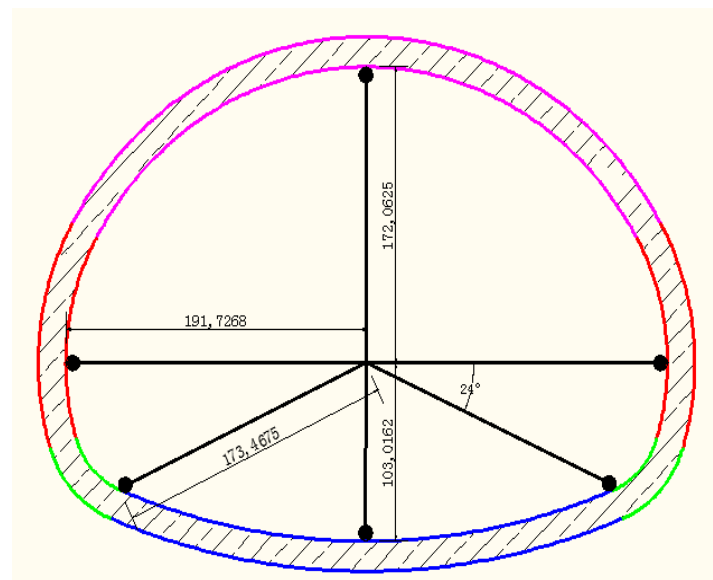


Figure 5. Layout plan of strain gauge measurement points with one percent accuracy (mm).

- (2) Contact pressure between the lining and surrounding rock

In order to measure the contact pressure between the surrounding rock and the lining, measuring points were set up at typical locations around the tunnel (crown, keystone, wall base, upward arch or pile intervals, pile top, etc.), and 13 miniature soil pressure boxes were buried between them. The specific method was to stick the soil pressure box in the

corresponding measuring point position before the lining was buried, as shown in Figure 6. The pressure boxes were buried in a cross-section 50 cm away from the tunnel entrance.

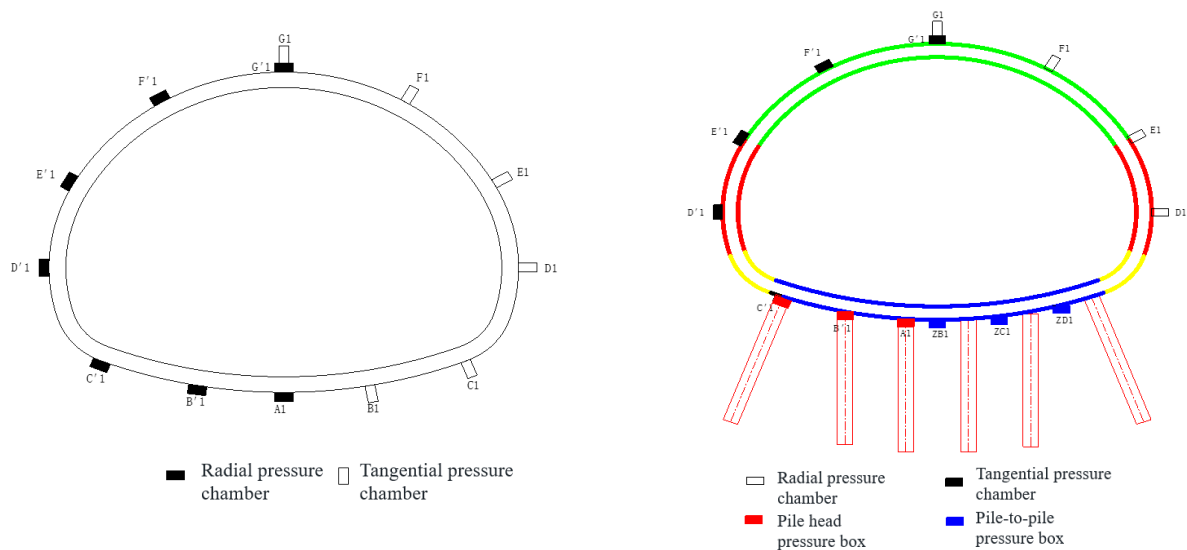


Figure 6. Schematic diagram of tunnel surrounding rock pressure monitoring.

(3) Water content of surrounding rock

Considering that the main purpose of the model test is to analyze the stress and deformation characteristics of the foundation after the surrounding rock is immersed in water, the immersion time was set to begin after the completion of tunnel excavation and the stress and deformation of the surrounding rock basically stabilized. Moisture content sensors were mainly installed at typical locations around the tunnel, and were densely arranged in the bottom and base soil of the upward arch according to the experimental purpose, with a measurement point interval of 0.25 m. They were buried in a section 70 cm away from the tunnel entrance, as shown in Figure 7.

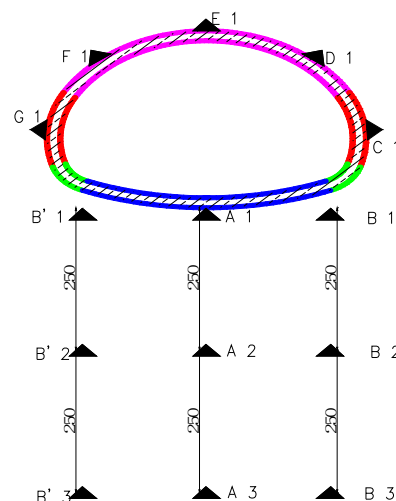


Figure 7. Schematic diagram for monitoring the moisture content of the substrate (mm).

(4) Stress in base soil

The stress sensors were resistance strain-type soil pressure boxes, which were densely arranged in the bottom and base soil of the upward arch according to the experimental purpose. The measurement point interval was 15 cm, and they were buried in a section 50 cm away from the tunnel entrance, as shown in Figure 8.

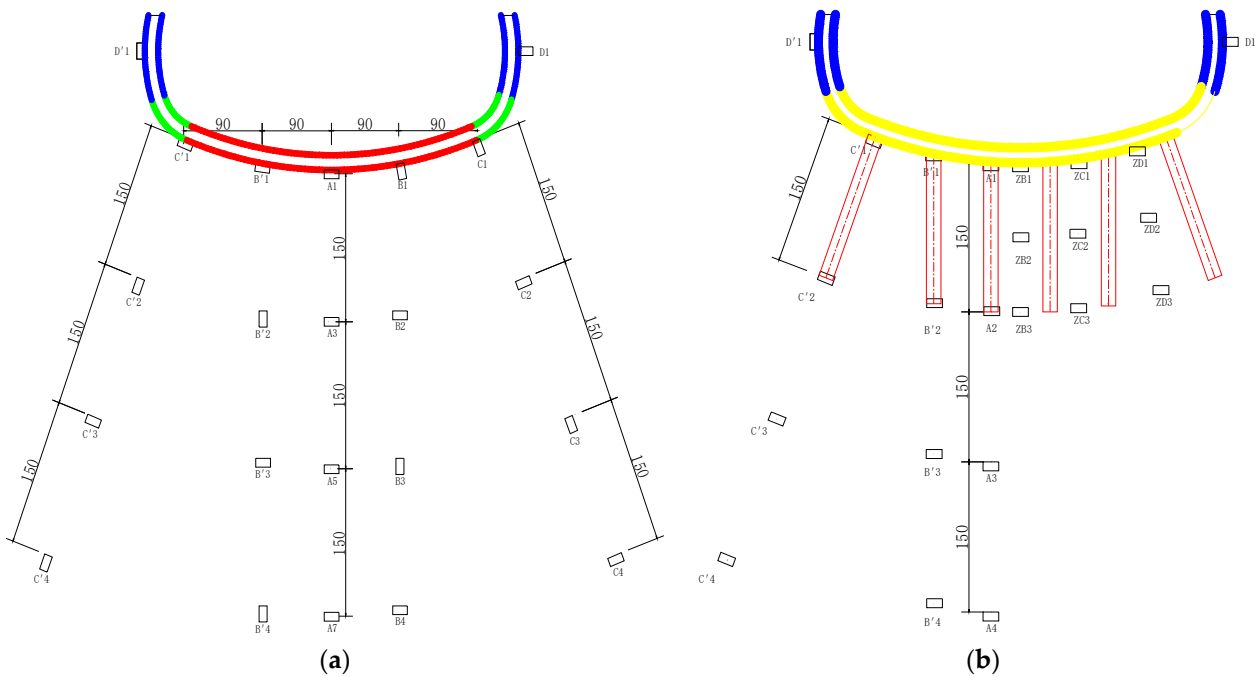


Figure 8. Schematic diagram of stress monitoring of foundation soil (mm). (a) Under natural foundation conditions; (b) rotary jet grouting pile reinforcement foundation.

(5) Foundation soil displacement

The settlement and deformation test of the tunnel model’s base soil will be measured using multi-point displacement meters. The specific method is to bury the sensor at different depths along the transverse section of the tunnel in order to obtain the overall deformation law of the base soil along the transverse section after the base soil is subjected to pressure from the tunnel. As shown in Figure 9, a layer of displacement meters is arranged every 30 cm at the base position, and they are buried in a section 30 cm away from the tunnel entrance.

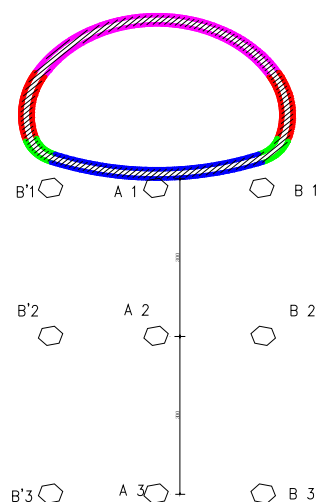


Figure 9. Cross-section diagram of displacement measurement points for foundation soil.

2.2.5. Basic Process of Model Test

The initial stress field inside the surrounding rock and the secondary stress distribution after excavation are key influencing factors in tunnel engineering. Therefore, it is particularly important for the model test to accurately simulate the initial stress field and

the secondary stress field after tunnel excavation. As the purpose of this model test is to study the stress and deformation characteristics of the tunnel base and surrounding rock under the conditions of the tunnel construction excavation process and initial support closure, a method was adopted wherein the surrounding rock was first filled up to below the upward arch, and a relatively hard soil was used to fill up the initial support model. Then, the entire surrounding rock was poured to the final elevation. In this way, the stress and deformation characteristics of the tunnel base and surrounding rock could be studied, and the deformation process of the tunnel lining structure could be observed while analyzing the interaction between the initial support and surrounding rock. The specific experimental steps are as follows:

- (1) Determine the similarity ratios of various physical parameters for the model test.
- (2) Based on the determined similarity ratios, prepare similar materials for the surrounding rock and lining structure, and determine the ratio and preparation method of similar materials for the surrounding rock, lining, and pile body that comply with the similarity theorem.
- (3) Model fabrication. When pasting and assembling the model, it is necessary to ensure that there are no bubbles between the two-ring models and that the pasting is firm. After the entire model is completed, it should be placed in a natural environment for seven days until the glue strength comes up before burial.
- (4) Install and test various instruments. Position displacement meters and strain-type soil pressure boxes according to the measurement point layout diagram. When arranging the displacement of the soil and the pressure measurement points of the surrounding rock, test wires should be arranged in an S-shape and numbered according to the test plan. After checking the quality of the strain-type pressure box and testing components, moisture-proof and protective measures should be taken for the displacement meters.
- (5) Surrounding rock filling. The surrounding rock is layered and filled with 6 cm each time. After smoothing, it is compacted with a 10 kg tamper. After each compaction, a sampling density measurement is taken with an environmental knife, and the density is strictly controlled to 1.52 g/cm^3 .
- (6) Pile embedding. The pile is embedded when the surrounding rock is filled to the elevation of the pile top. Pile embedding is divided into four processes: hole drilling, grouting, pile placement, and grouting filling. The hole depth and direction need to be controlled, and disturbance to the surrounding soil should be minimized during the hole drilling process. Grouting is performed to ensure a tight integration between the pile and the surrounding soil when placing the pile. Grout filling is necessary to ensure a tight integration between the pile body and the soil.
- (7) Support process. Due to the small operating space of the model test, it is difficult to support while excavating, so simplified support is used, and pre-embedding is used to simulate the support process. The rock filling stops at 20 cm above the base elevation, and according to the tunnel excavation position and cross-sectional shape, a trench is excavated to ensure that the tunnel lining base is in close contact with the trench bottom. To simulate the soil excavation process, the lining structure needs to be filled with soil. Wet sand and loess are mixed evenly at a ratio of 1:2 to minimize deformation caused by pre-embedding, and they are layered and tamped into the lining. After tamping, the entire lining is placed into the excavated trench, and then the surrounding rock is poured.

3. Similarity Theory

3.1. Study Using the Dimensional Analysis Method

If there are similar systems, under the condition of geometric similarity and only considering self-weight effects, the stress and strain of these two similar systems should have the following relationship. Among them, the Calculation table of similarity constants for physical quantities can be found in Table 2.

Table 2. Calculation table of similarity constants for physical quantities.

Physical Quantity	Symbol	Gravity Unit Coefficient	Absolute Unit Coefficient	Generic Relationship	Strict Similarity
Length	L	L	L	C_l	C_l
Time	t	T	T	C_t	C_t
Density	ρ	$FL^{-1}T^2$	mL^{-3}	$C_p = C_F C_l^{-4} C_t^2 =$ $C_m C_l^{-3} = C_\gamma C_l^{-1} C_t^2$	$C_p = C_F C_l^{-3} =$ $C_m C_l^{-3} = C_\gamma$
Quality	m	$FL^{-1}T^{-2}$	m	$C_m = C_F C_l^{-1} C_t^2 =$ $C_p C_l^3 = C_\gamma C_l^2 C_t^2$	$C_m = C_F = C_p C_l^3$
Power	F	F	mLT^{-2}	$C_F = C_m C_l^{-1} C_t^{-2} =$ $C_p C_l^4 C_t^{-2} = C_\gamma C_l^3$	$C_F = C_m = C_p C_l^3$
Unit weight	$\varepsilon(\gamma)$	FL^{-3}	$mL^{-2}T^2$	$C_p = C_F C_l^{-4} C_t^2 =$ $C_m C_l^{-3} = C_\gamma C_l^{-1} C_t^2$	$C_\gamma = C_p$
Stress intensity	σ	FL^{-2}	$mL^{-1}T^2$	$C_\sigma = C_p = C_c =$ $C_E C_\varepsilon C_F C_l^{-2} = C_\gamma C_l$	$C_\sigma = C_E = C_p C_l$
Adhesive force	c				
Elastic modulus	E	FL^{-2}	$mL^{-1}T^2$	$C_E = C_F C_l^{-2} C_\varepsilon^{-1}$ $= C_\gamma C_l C_\varepsilon^{-1}$	$C_E = C_\sigma = C_p C_l$
Shear modulus	G	FL^{-2}	$mL^{-1}T^2$	$C_G = C_\lambda C_l C_\varepsilon^{-1}$	$C_G = C_\sigma = C_p C_l$
Poisson’s ratio	ν	Dimensionless	Dimensionless	$C_\nu = 1$	$C_\nu = 1$
Frictional coefficient	f	Dimensionless	Dimensionless	$C_f = 1$	$C_f = 1$
Gravitational acceleration	g	LT^2	LT^2	$C_g = C_l C_t^{-2}$	$C_g = 1$

The physical quantities considered in the system include geometric dimensions l , unit weight of materials γ , elastic modulus E of materials, Poisson’s ratio ν , stress σ , and strain ε . The equation relating these quantities is:

$$f(\sigma, E, l, \gamma, \nu, \varepsilon) = 0 \tag{1}$$

According to the Pi theorem, Poisson’s ratio ν and strain ε are dimensionless quantities and are thus similarity constants for the system. Choosing m, L , and T as the basic units, the dimensional matrix of the equation is:

	σ	E	γ	l
m	1	1	1	0
L	-1	-1	-2	1
T	-2	-2	-2	0

There are only 2 independent physical quantities, so the number of similarity criteria is 2. Selecting geometric dimension l and unit weight of materials γ as the two physical quantities, according to dimensional analysis:

$$\pi_1 = \frac{\sigma}{\gamma \cdot l}, \pi_2 = \frac{E}{\gamma \cdot l} \tag{2}$$

Therefore, the following similarity indices can be obtained:

$$C_\sigma = C_l \cdot C_\gamma, C_E = C_E, C_\nu = 1, C_\varepsilon = 1 \tag{3}$$

3.2. Similarity Criteria for Lining Structures

For lining structures, the main controlling factors for safety are the flexural capacity and bending strain. Therefore, the similarity model should mainly focus on flexural stiffness. The tunnel lining can be viewed as a thin plate structure, and the similarity ratio can be derived using the control equation for thin plate bending. According to the differential equation for thin plate bending in elastic–plastic mechanics [20],

$$\nabla^2 \nabla^2 w = \frac{q}{Q} \quad (4)$$

The expansion form in the Cartesian coordinate system is:

$$\frac{\partial^4 w}{\partial x_1^4} + 2 \frac{\partial^4 w}{\partial x_1^2 \partial y^2} + \frac{\partial^4 w}{\partial x_2^4} = \frac{q}{Q} \quad (5)$$

Let h be the thickness of the plate, and x and y be the two mutually perpendicular coordinates. The uniformly distributed transverse load is q , the deflection of the thin plate is w , and the flexural rigidity is Q . Then, the equation becomes:

$$\frac{\partial^4 w}{\partial x^4} + 2 \frac{\partial^4 w}{\partial x^2 \partial y^2} + \frac{\partial^4 w}{\partial y^4} = \frac{q}{Q} \quad (6)$$

In the equation, Q can be expressed as:

$$Q = \frac{Eh^3}{12(1-\nu^2)} \quad (7)$$

In the equation, E represents elastic modulus and ν represents Poisson's ratio. The corresponding equations for the prototype and model (with subscripts p and m denoting prototype and model, respectively) are as follows:

$$\left. \begin{aligned} \frac{\partial^4 w_p}{\partial x_p^4} + 2 \frac{\partial^4 w_p}{\partial x_p^2 \partial y_p^2} + \frac{\partial^4 w_p}{\partial y_p^4} &= \frac{q_p}{Q_p} \\ \frac{\partial^4 w_m}{\partial x_m^4} + 2 \frac{\partial^4 w_m}{\partial x_m^2 \partial y_m^2} + \frac{\partial^4 w_m}{\partial y_m^4} &= \frac{q_m}{Q_m} \end{aligned} \right\} \quad (8)$$

Substituting the similarity relationship into Equation (8), we obtain:

$$\frac{c_w}{c_l^4} \left(\frac{\partial^4 w_p}{\partial x_p^4} + 2 \frac{\partial^4 w_p}{\partial x_p^2 \partial y_p^2} + \frac{\partial^4 w_p}{\partial y_p^4} \right) = \frac{c_p}{c_Q} \frac{q_p}{Q_p} \quad (9)$$

Comparing Equation (8) with Equation (9), we know that:

$$c_w c_Q = c_q c_l^4 \quad (10)$$

In the model testing of underground structures that can be restored in a gravity field, since $c_q = 1$ and $c_w = c_l$, Equation (10) yields:

$$c_Q = c_l^3 \quad (11)$$

Let the constant of geometric similarity be $c_l = \frac{1}{n}$, then:

$$Q_m = \frac{1}{n^3} Q_p \quad (12)$$

Substituting (7) into (12), we get:

$$n^3 \frac{h_m^3}{h_p^3} = \frac{E_p (1-\nu_m^2)}{E_m (1-\nu_p^2)} \quad (13)$$

If $a = b$ and $b = c$, then Equation (13) can be simplified as:

$$h_m = \frac{h_p}{n} \quad (14)$$

But the material of the selected model is not identical to that of the prototype, i.e., $E_p \neq E_m$ and $\nu_p \neq \nu_m$ do not hold.

$$h_m = \frac{h_p}{n} \left[\frac{E_p (1 - \nu_m^2)}{E_m (1 - \nu_p^2)} \right]^{1/3} \quad (15)$$

Based on Equation (15), the thickness of the lining structure of the model can be obtained.

According to the stress expression for thin plate bending in elastoplastic mechanics:

$$\sigma_x = -\frac{E_z}{1 - \nu^2} \left(\frac{\partial^2 w}{\partial x^2} + \mu \frac{\partial^2 w}{\partial y^2} \right) \quad (16)$$

$$\sigma_y = -\frac{E_z}{1 - \nu^2} \left(\frac{\partial^2 w}{\partial y^2} + \mu \frac{\partial^2 w}{\partial x^2} \right) \quad (17)$$

$$\tau_{xy} = -\frac{E_z}{1 + \nu} \frac{\partial^2 w}{\partial x \partial y} \quad (18)$$

In the equation, z represents the coordinate in the thickness direction of the plate. Using the same method as above, we can obtain the stress of the prototype:

$$\sigma_p = \frac{h_p}{nh_m} \frac{E_p}{E_m} \sigma_m \quad (19)$$

The stress of the prototype in the model inference can be obtained by Equations (16)–(18):

$$\sigma_p = \frac{1 - \nu_p^2}{1 - \nu_m^2} \left(\frac{nh_m}{h_p} \right)^2 \sigma_m \quad (20)$$

4. Model Experiment Design

4.1. Production of Pits and Grooves

In line with the objective of experimental research, a dedicated model test platform was established using a model test pit with dimensions of 2.50 m × 1 m × 4 m (tunnel transverse × tunnel longitudinal × depth), and the model test body was constrained by a 370 mm-thick brick–concrete structure and a square steel glass barrier wall. The glass used was 15 mm tempered glass, and the glass barrier wall was constructed by bonding structural glass glue to a square steel frame. The bottom of the model test pit was cast with concrete, and the pit walls were constructed with 370 mm brick–concrete walls and finished with cement smoothing. One side of the square steel–glass barrier wall was located at the tunnel excavation entrance, which allowed for convenient observation and monitoring of changes in the surrounding rock during testing. In order to facilitate the installation of the square steel–glass barrier wall, four pieces were installed in total, with the tunnel opening reserved at a height of 1 m from the bottom of the pit, as shown in Figure 10. The completed model test pit is shown in Figure 11.

Through model immersion tests, it is possible to gain a more intuitive understanding of the deformation and base displacement stress changes of large cross-section loess tunnels under adverse conditions.

Water is allowed to infiltrate into the surrounding rock through soil pores and cracks by using a seepage method until the soil is saturated. Seepage begins after the deformation of the surrounding rock stabilizes following excavation completion and ends after the soil is fully saturated. This process is illustrated in Figure 12.



Figure 10. Production of model test pits. (a) Test pit; (b) Pit side support frame; (c) Tempered glass; (d) Square steel glass retaining wall.

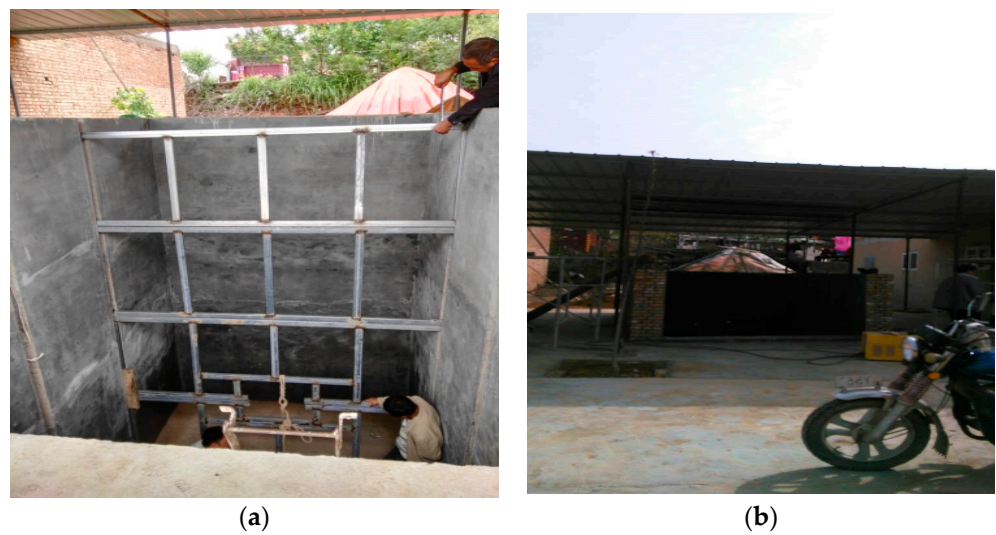


Figure 11. Model test pit and canopy. (a) Frame test slot; (b) Canopy.



Figure 12. Immersion process.

4.2. Selection of Similar Materials for the Model

4.2.1. Model Test Similarity Ratio

When selecting the model scale, two factors should be considered: (1) measurement accuracy requirements and (2) experimental equipment conditions. Regarding measurement accuracy, the strain values of most measuring points in the model should be kept within the optimal range of the strain gauge [21]. For experimental equipment conditions, it is necessary to estimate that the maximum strain and displacement values of the model should not exceed the range of the testing element, in addition to meeting the accuracy requirements. Furthermore, it is essential to consider whether the loading conditions and experimental platform can meet the experimental requirements. In choosing the model scale, besides considering the measurement and loading conditions, it is also necessary to take into account the cost of the experiment. Generally, the larger the model scale, the higher the precision, but this also requires more cost and time. On the other hand, small-scale model production costs are low, and the testing period is short. For underground chamber planar models, the scale used is usually between 1/50 and 1/200. In principle, the simulation range for model testing should include the area affected by the structural load. Generally, the boundary of the tunnel chamber should be larger than three times its diameter. From the overall intention of this study, a large geometric scale model was adopted for this model test.

Geometric similarity ratio: based on the site conditions, experimental site, and limitations of the experiment itself, we determined the geometric size ratio of the model to be 1:40. Therefore, the geometric similarity constant is $C_l = 40$.

Gravity similarity ratio and strength similarity ratio: based on previous research experience, the gravity of similar materials can generally be controlled within a large range. For the sake of calculation convenience, the gravity similarity ratio C_γ between the prototype and model can be taken as 1.

According to the similarity principle, the similarity constant of strength indicators (including elastic modulus, cohesive force, and compressive strength) is equal to the product of the geometric similarity constant C_l and gravitational similarity constant C_γ , that is, $C_\sigma = C_\gamma \cdot C_l$.

Geometric similarity ratio: $C_l = 40$.

- (1) Gravity similarity ratio: $C_\gamma = 1$;
- (2) Poisson's ratio, strain, and friction angle similarity ratio: $C_\nu = C_\epsilon = C_\phi = 1$;
- (3) Strength, stress, cohesion, and elastic modulus similarity ratio: $C_R = C_\sigma = C_c = C_E = 40$.

While satisfying the similarity conditions specified by the third theorem as much as possible, the main factors that play a role should be grasped, minor factors should be omitted, and the primary similarity conditions should be maintained to obtain an approximate similarity that is sufficiently accurate in practice. The main mechanical parameters of the model following the above similarity relationship are set as follows [21–24]:

- (1) Surrounding rock: Unit weight $\gamma = 1.52 \text{ g/cm}^3$, elastic modulus $E = 1.3 \text{ MPa}$, Poisson's ratio $\nu = 0.3$. Shrinkage coefficient $\delta_s = 0.043$.
- (2) Modeled concrete and sprayed concrete: Elastic modulus $E = 3300 \text{ MPa}$, Poisson's ratio $\nu = 0.38$, thickness $h = 15 \text{ mm}$;
- (3) Spinning jet pile: Elastic modulus $E = 260 \text{ MPa}$, Poisson's ratio $\nu = 0.22$.

4.2.2. Selection and Preparation of Materials for Surrounding Rock Model Test

A mixture of barite powder, bentonite, industrial salt, gypsum, and standard sand in a ratio of 8:12:45:25:10 was selected and stirred to control the shrinkage coefficient δ_s within 0.043. Figure 13a,b shows indoor blending and indoor slurry tests, respectively. Layered filling was used, with each layer filled to a depth of 6 cm and leveled using a horizontal ruler (as shown in Figure 13b). After leveling, a 10 kg weight was used to compact the layer repeatedly with an environmental knife being used to take samples for density testing after each compaction until the required density was achieved. Table 3 lists the mechanical parameters of rock and model materials. Figure 13c shows the process of compacting the surrounding rock, while Figure 13d shows the process of taking density samples using an environmental knife.



Figure 13. Material selection and preparation. (a) Indoor mixing; (b) Indoor wetting test; (c) Compaction process; (d) Sampling with a ring knife.

Table 3. Mechanical parameters of surrounding rock and model materials.

Material	Elastic Modulus E (MPa)	Poisson's Ratio ν	Severe γ kN/cm ³	Coefficient of Collapsibility δ_s
Prototype materials	52	0.3	15.2	0.043
Modeling materials	1.3	0.3	15.2	0.043

4.2.3. Selection and Preparation of Lining Similar Materials

For the simulation of initial support, due to the large scale of the similar model, it is difficult or even impossible to produce similar simulated supports and structures by scaling down prototype materials according to geometric similarity ratios. Even if they are manufactured, it will lead to distortions in the simulation effect. The current solution for such problems is to use the equivalent stiffness method for conversion simulation [25]. In the construction process of the tunnel, the support and structure are classified according to the stress state, and the bending stiffness should be taken as a comprehensive quantity in the simulation of the support body, such as steel frames and concrete linings, which mainly bear bending force, to be equivalent to the stiffness in the model.

For the support design of Class V surrounding rock in large-section loess tunnels, a combined support system of steel and shotcrete is adopted. The initial lining thickness of the prototype tunnel is 30 cm, with C25 concrete and HW175 steel support with a longitudinal spacing of 60 cm. $\Phi 22$ steel bars are used to connect each steel arch, and the circumferential spacing is 1 m, with 30 cm of C25 shotcrete. The elastic modulus of the initial support in the prototype can be calculated according to the following formula:

$$E = E_0 + \frac{S_g \times E_g}{S_c} + \frac{S_b \times E_g}{S_c} \quad (21)$$

$$\gamma = \frac{\gamma_g \times L \times S_g + \gamma_c \times (a \times b \times L - S_g \times L - 8S_b \times L) + 8\gamma_b \times L}{a \times b \times L} \quad (22)$$

wheres,

E is the converted elastic modulus of the shotcrete;

E_0 is the original elastic modulus of the shotcrete;

S_g is the cross-sectional area of the steel arch;

E_g is the elastic modulus of the steel;

S_c is the cross-sectional area of the shotcrete;

S_b is the cross-sectional area of the steel mesh;

γ_g is the weight of the steel arch;

γ_c is the weight of the shotcrete;

γ_b is the weight of the steel mesh;

L is the unit length.

Gypsum is a brittle material with properties similar to concrete. However, since gypsum loses strength when exposed to water, it is not suitable for lining structures in this study. Organic glass is an isotropic homogeneous material that is easy to process using woodworking tools. As the material is transparent, any defects in the connections can be immediately detected. Additionally, organic glass features high strength and low elasticity, making it ideal for simulating the deformation of lining structures under stress. Using electrical measurement, the elastic modulus of the organic glass was found to be $E = 3300$ MPa and the Poisson's ratio $\nu = 0.38$ through uniaxial compression testing indoors. According to the similarity formula, its thickness was calculated to be 15 mm. Figure 14 shows the standard sample of the organic glass, while Figure 15 shows the similar model of the lining structure. A layer of frosted adhesive tape was applied to the outer surface of the lining to increase the contact force between the lining and the soil. Table 4 shows the mechanical parameter indicators for the prototype and model materials, with anti-bending stiffness as the main control indicator for scaling.



Figure 14. Standard Sample of Organic Glass.



Figure 15. Similar Model of Lining Structure.

Table 4. Mechanical parameters of lining structure prototype and model materials.

Material	Elastic Modulus E (MPa)	Poisson's Ratio ν	Compressive Strength R_c MPa
Prototype materials	29,500	0.22	25
Modeling materials	3300	0.38	25

4.2.4. Selection of Material for Rotary Spray Pile Body Model and Preparation of Model Piles

In order to maximize the strain value of the pile body in the experiment, while ensuring that the pile body itself does not undergo damage, it is required that the stiffness of the model pile used in the experiment should not be too high, but its strength cannot be too low [26]. Based on the size of the model groove and after considering the feasibility of the production process, the model pile used in the experiment was made by mixing cement and fine-grained cohesive soil in a certain proportion with water. The material for the pile body model can use cement with the label number P·O·32.5, and yellow clay with a grain size below 1 mm mixed with water in a certain proportion taking the elastic modulus as the control indicator according to Table 5.

Table 5. Mechanical parameters of prototype and model materials for rotary spray piles.

Material	Elastic Modulus E (MPa)	Poisson's Ratio ν	Compressive Strength R_c (MPa)
Prototype materials	10,400	0.25	12.5
Modeling materials	260	0.25	0.315

The similar material for rotary spray piles is prepared by mixing cement with a label number of P·O·32.5 and yellow clay in a certain water–cement ratio and stirred uniformly. The preparation of the similar material for rotary spray piles takes the elastic modulus as the main control indicator. The selected P·O·32.5 cement is mixed with yellow clay in the ratio shown in Table 5, weighed in a sealed container, mixed with water, and poured into a cylindrical mold with a diameter of 5 cm and a height of 10 cm, and a square mold with a length of 7.6 cm to make a geotechnical experiment specimen. After being cured under natural conditions for one day, the specimens can be demolded. After demolding, they are cured in a standard curing box for 28 days, and their compressive strength and elastic modulus are measured using a universal testing machine, as shown in Figure 16. Table 6 shows the results of indoor test measurements.



Figure 16. Lining material test. (a) Compressive strength test; (b) Elastic modulus test.

According to Table 6, the compressive strength and elastic modulus of S1~S4 gradually decrease. Based on the theory of similarity and taking the elastic modulus as the main control indicator, S4 was finally selected as the optimal ratio. The model pile is made by using a prefabrication method. After preparing the slurry according to the selected ratio and mixing it with yellow clay in a certain proportion, it is poured into a mold tube with a diameter of 15 mm, fully vibrated, and can avoid voids in the pile body. After being placed

under natural conditions for one day, the model pile can be demolded. Then, it is immersed in water for 28 days for curing, and the pile is completed at this point.

Table 6. Proportion and physical parameters of rotary spray piles.

Number	Water-Cement Ratio	Loess Content in Rotary Jet Grouting Piles (%)	Material Mass Ratio			Compressive Strength (MPa)	Elastic Modulus (MPa)
			Cement	Water	Loess		
S 1	1:1	50	1	1	2	2.86	328
S 2	1:1	55	1	1	2.33	2.53	301
S 3	1:1	60	1	1	3	2.14	286
S 4	1:1	65	1	1	3.71	1.71	259
S 5	1:1	70	1	1	4.67	1.32	212

5. Conclusions

Starting from the theory of similarity, this paper determines the similarity ratio, selects similar materials and control indicators through indoor experiments, and formulates specific experimental plans. The conclusions are as follows:

1. The geometric similarity ratio was determined to be 1:40, allowing for the creation of scaled models of the surrounding rock and lining materials. By using appropriate materials and proportions, the models accurately simulate the stress and deformation characteristics of tunnel engineering.
2. The control of the wetting settlement coefficient, δ_s , within 0.043 ensures the stability and reliability of the chosen rock materials. The selection of materials such as barite powder, bentonite, industrial salt, gypsum, and standard sand, mixed in percentages of 8:12:45:25:10, respectively, guarantees the proper behavior and mechanical properties of the rock models.
3. Organic glass was chosen as the material for the lining structure, with the bending stiffness EI and Poisson's ratio μ acting as control indicators during determination. This selection is based on an understanding of the stress and deformation behavior of the lining structure in practical engineering. By controlling the bending stiffness and Poisson's ratio of the material, the mechanical characteristics of the lining structure can be accurately simulated and its performance and interaction with the surrounding rock can be studied.

During the testing process, the surrounding rock was first filled up to the crown level, followed by the placement of a relatively hard soil inside the initial support model. Finally, the entire surrounding rock was poured until reaching the final elevation, simulating the construction process of a real tunnel. Through this test scheme, a comprehensive analysis of stress, deformations, and the interaction between the initial support and surrounding rock could be conducted, providing valuable insights for optimizing the design and construction of tunnel engineering projects.

Author Contributions: Writing—original draft, Z.L.; Software, S.L.; Investigation, J.Z.; Resources, L.L.; Methodology, K.H. All authors have read and agreed to the published version of the manuscript.

Funding: This research received no external funding.

Data Availability Statement: We declare that we have no financial and personal relationships with other people or organizations that can inappropriately influence our work, there is no professional or other personal interest of any nature or kind in any product, service, and/or company that could be construed as influencing the position presented in, or the review of, the manuscript entitled.

Conflicts of Interest: The authors declare no conflict of interest.

References

1. Shao, S.; Shao, S.; Li, J.; Qiu, B. An analysis of Loess Tunnel Failure and Its Mechanism. *Adv. Civ. Eng.* **2021**, *2021*, 6671666. [[CrossRef](#)]
2. Qiu, J.; Fan, F.; Zhang, C.; Lai, J.; Wang, K.; Niu, F. Response mechanism of metro tunnel structure under local collapse in loess strata. *Environ. Earth Sci.* **2022**, *81*, 164. [[CrossRef](#)]
3. Cheng, X.; Feng, H.; Qi, S.; Zhang, X.; Liu, B. Dynamic response of curved wall LTSLS under the interaction of rainwater seepage and earthquake. *Geotech. Geol. Eng.* **2017**, *35*, 903–914. [[CrossRef](#)]
4. Weng, X.; Zhou, R.; Rao, W.; Wang, D. Research on subway shield tunnel induced by local water immersion of collapsible loess. *Nat. Hazards* **2021**, *108*, 1197–1219. [[CrossRef](#)]
5. Zucca, M.; Valente, M. On the limitations of decoupled approach for the seismic behaviour evaluation of shallow multi-propped underground structures embedded in granular soils. *Eng. Struct.* **2020**, *211*, 110497. [[CrossRef](#)]
6. Xue, Y.; Ma, X.; Yang, W.; Ma, L.; Qiu, D.; Li, Z.; Zhou, B. Total deformation prediction of the typical loess tunnels. *Bull. Eng. Geol. Environ.* **2020**, *79*, 3621–3634. [[CrossRef](#)]
7. Hongtao, N.; Shengjun, S.; Xin, Z. Study on failure characteristics of surrounding rock of benching excavation in loess overburden soil-rock contact zone. *Earth Sci. Inform.* **2022**, *15*, 1879–1887. [[CrossRef](#)]
8. Savvides, A.-A.; Papadopoulos, L. A Neural Network Model for Estimation of Failure Stresses and Strains in Cohesive Soils. *Geotechnics* **2022**, *2*, 1084–1108. [[CrossRef](#)]
9. Sun, Z.; Yang, X.; Lu, S.; Chen, Y.; Li, P. Influence of a Landslide on a Tunnel in Loess-Bedrock Ground. *Appl. Sci.* **2022**, *12*, 6750. [[CrossRef](#)]
10. Mao, Z.; Wang, X.; An, N.; Li, X.; Wei, R. Water disaster susceptible areas in loess multi-arch tunnel construction under the lateral recharge condition. *KSCE J. Civ. Eng.* **2019**, *23*, 4564–4577. [[CrossRef](#)]
11. Liu, Y.; Lai, H.; Xie, Y.; Song, W. Cracks analysis of highway tunnel lining in flooded loess. *Proc. Inst. Civ. Eng. Geotech. Eng.* **2017**, *170*, 62–72. [[CrossRef](#)]
12. Fumagalli, E. *Statical and Geomechanical Models*; Springer Science & Business Media: Berlin/Heidelberg, Germany, 2013.
13. Fan, H.; Xu, Q.; Lai, J.; Liu, T.; Zhu, Z.; Zhu, Y.; Gao, X. Stability of the loess tunnel foundation reinforced by jet grouting piles and the influence of reinforcement parameters. *Transp. Geotech.* **2023**, *40*, 100965. [[CrossRef](#)]
14. Cheng, X.; Zhou, X.; Liu, H.; Zhou, Y.; Shi, W. Numerical analysis and shaking table test of seismic response of tunnel in a loess soil considering rainfall and traffic load. *Rock Mech. Rock Eng.* **2021**, *54*, 1005–1025. [[CrossRef](#)]
15. Qiu, J.; Lu, Y.; Lai, J.; Guo, C.; Wang, K. Failure behavior investigation of loess metro tunnel under local-high-pressure water environment. *Eng. Fail. Anal.* **2020**, *115*, 104631. [[CrossRef](#)]
16. Cheng, X.; Zhou, X.; Shi, W. Dynamic responses of loess tunnels with different cross sections under the action of earthquakes, rainwater seepage and trains. *J. Vibroeng.* **2020**, *22*, 1427–1452. [[CrossRef](#)]
17. Lai, H.; Zhang, J.; Zhang, L.; Chen, R.; Yang, W. A new method based on centrifuge model test for evaluating ground settlement induced by tunneling. *KSCE J. Civ. Eng.* **2019**, *23*, 2426–2436. [[CrossRef](#)]
18. Fan, H.; Liu, T.; Zhang, S.; He, H.; Zhu, Z.; Zhu, Y.; Gao, X. Effects of Jet-Grouting Piles on Loess Tunnel Foundation with Centrifugal Model Tests. *Int. J. Geomech.* **2023**, *23*, 04022298. [[CrossRef](#)]
19. Yang, T.; Zhang, J.; Zhang, X.; Zhang, Q.; Yin, Z. Layered grouting technology based on a comprehensive water-to-cement ratio for the overlying loess stratum of urban shallow tunnels. *Adv. Civ. Eng.* **2020**, *2020*, 2904789. [[CrossRef](#)]
20. Tian, Q.; Zhang, J.; Zhang, Y. Similar simulation experiment of expressway tunnel in karst area. *Constr. Build. Mater.* **2018**, *176*, 1–13. [[CrossRef](#)]
21. Huang, B. *Model Test and Numerical Simulation Research on the Failure Mechanism of a Single-Arch Four-Lane Highway Tunnel*; Central South University: Changsha, China, 2010.
22. Tian, Z.Y. *Model Test Study on Small Clearance Distance of Highway Tunnel*; Southwest Jiaotong University: Changsha, China, 2006.
23. Zhao, G. *Model Test Study on Double-Arch Tunnel*; Southwest Jiaotong University: Changsha, China, 2005.
24. Cheng, F.H. *Model Test and Field Test Study on the Influence of Spacing between Two Parallel Eight-Lane Highway Tunnels*; Southwest Jiaotong University: Changsha, China, 2011.
25. Wu, B.; Xu, G.; Shing, P.B. Equivalent force control method for real-time testing of nonlinear structures. *J. Earthq. Eng.* **2011**, *15*, 143–164. [[CrossRef](#)]
26. Liu, L.; Li, Z.; Liu, X.; Li, Y. Frost front research of a cold-region tunnel considering ventilation based on a physical model test. *Tunn. Undergr. Space Technol.* **2018**, *77*, 261–279. [[CrossRef](#)]

Disclaimer/Publisher's Note: The statements, opinions and data contained in all publications are solely those of the individual author(s) and contributor(s) and not of MDPI and/or the editor(s). MDPI and/or the editor(s) disclaim responsibility for any injury to people or property resulting from any ideas, methods, instructions or products referred to in the content.